# Determination of mass diffusion overpotential distribution with flow pulse method from current distribution measurements in a PEMFC

M. NOPONEN*, T. HOTTINEN, T. MENNOLA, M. MIKKOLA and P. LUND
*Helsinki University of Technology, Laboratory of Advanced Energy Systems, PO Box 2200, 02015 HUT, Finland*
*(*author for correspondence: fax: +358 9 451 3195, e-mail: matti.noponen@hut.fi)*

## Abstract

The mass diffusion overpotential distribution in a free-breathing proton exchange membrane fuel cell (PEMFC) was determined from current distribution measurements using a flow pulse approach. The current distribution measurements were conducted with a segmented flow-field plate. Flow pulses were fed to the cathode channels to form a uniform oxygen concentration distribution along the channels. Simultaneously, the cell resistance was monitored using the current interruption method. From the experimental data, the mass diffusion overpotential distribution was calculated using the Tafel equation. The results show that the mass diffusion overpotential in different parts of the cell may vary considerably, for example, at 180 mA cm$^{-2}$ the mass diffusion overpotential difference between the bottom and top part of the cell was 0.1 V.

## List of symbols

| | |
|---|---|
| $E$ | cell potential (V) |
| $E_{rev}$ | cell reversible potential (V) |
| $E_0$ | open circuit potential (V) |
| $\eta$ | overpotential (V) |
| $b$ | Tafel slope (V dec$^{-1}$) |
| $i_0$ | exchange current density (A cm$^{-2}$) |
| $i$ | current density (A cm$^{-2}$) |
| $I$ | current (A) |
| $r$ | sum of all linear overpotentials ($\Omega$ cm$^2$) |
| $C$ | concentration (mol m$^{-3}$) |
| $R$ | area specific resistance ($\Omega$ cm$^2$) |
| $\mathscr{R}$ | gas constant (8.314 J mol$^{-1}$ K$^{-1}$) |
| $T$ | temperature (K) |
| $\mathscr{F}$ | Faraday's constant (96 485 C mol$^{-1}$) |
| $MBD$ | relative mean bias difference |
| $RMSD$ | relative root mean square difference |
| $n$ | number of data points |

*Subscripts/superscripts*

| | |
|---|---|
| c | cathode |
| conc | concentration |
| hom | homogenized oxygen concentration |
| ref | reference value |
| calc | calculated value |
| meas | measured value |
| j | element of a matrix |
| O$_2$ | oxygen |

## 1. Introduction

Small fuel cells may offer an interesting alternative to batteries in providing power to small electronic devices. To maximize the efficiency of a fuel cell system, the power consumption of auxiliary devices (e.g., fans, compressors and mass flow controllers) has to be minimized. At the cathode side, oxygen delivery by free convection may therefore be advantageous.

The use of natural circulation of oxidant and fuel makes the designing of the cell more complicated because special attention has to be given to the minimization of the mass diffusion overpotential. However, the direct measurement of the mass diffusion overpotential is a complex task because it is spatially varying in the active cell area. There are at least two alternatives to measure the distribution: the current distribution mapping and the spatial measurement of the concentration of oxidant and fuel. In addition, theoretical models (e.g., [1, 2]), can be used to evaluate the effect of the mass diffusion losses.

Although quite a few experiments have been made on the determination of current distribution [3–10], no measurements have been made to determine the magnitude of the mass diffusion overpotential. We chose a hydrogen-fuelled PEMFC in which the mass diffusion losses on the anode side are usually negligible and, therefore, the measurements yield directly the mass diffusion losses of the cathode.

## 2. Experimental details

### 2.1. *Flow pulse approach*

Uneven current distributions are mainly caused by the nonuniform oxygen concentration inside the fuel cell. If the direction of the total water flux through the membrane is from the cathode to the anode, the hydrogen concentration may also vary resulting in uneven current distribution. This results from the reduction of the hydrogen partial pressure. However, when pure hydrogen is used the effect of the mass diffusion overpotential at the anode is usually minor compared to that on the cathode.

A flow pulse approach was developed to determine the mass diffusion overpotential distribution. The measurements were performed using a segmented cell, reported in detail in [10]. In addition, the total resistance of the cell was measured with the current interruption method.

On the one hand, because the segments of the flow-field plate are all at the same potential, the current interruption method alone cannot be used to investigate the resistances of each segment. On the other hand, if the concentration profile can be equalized throughout the cathode, the resistance of each segment can be calculated when the total resistance of the unit cell is known.

The polarization behaviour of a PEMFC can be modelled with the Tafel equation. By adding the anode side activation, ohmic and mass diffusion overpotentials into the formula, one can obtain the polarization behaviour for each segment j at the cathode side:

$$E = E_0 - b\ln(i_j) - r_j i_j - \eta_{conc,j} \tag{1}$$

where

$$E_0 = E_{rev} + b\ln(i_{0,c}) \tag{2}$$

and

$$\eta_{conc,j} = \frac{\mathscr{R}T}{2\mathscr{F}}\ln\left[\frac{C_j^{O_2}}{C_{ref}^{O_2}}\right] \tag{3}$$

When the concentration profile is uniform, Equation 1 reduces to

$$E_{hom} = E_0 - b\ln(i_{hom,j}) - r_j i_{hom,j} \tag{4}$$

This results from the assumption that the concentration temporarily achieves the reference value when a flow pulse is fed to the cathode channels. It is also assumed that the exchange current density and the activation energies are not dependent on oxygen concentration. By subtracting Equation 1 from Equation 4 the magnitude of the mass diffusion overpotential resulting from nonuniform oxygen concentration is obtained. To en-

sure that the oxygen concentration along the reaction surface is uniform, the flow pulse has to be strongly over stoichiometric and long enough to remove all excess water from the electrodes. On the other hand, the duration of the flow pulse has to be short enough in order not to change the resistance of the proton conductive phases of the MEA.

After a flow pulse is fed to the cathode channels, the oxygen concentration should be uniform and only the resistances of the cell segments cause variation in the current distribution profile. Because all segments are at the same potential and the segments are connected in parallel, the total resistance (R) can be calculated from the individual resistances ($R_j$) as

$$\frac{1}{R} = \sum \frac{1}{R_j} \tag{5}$$

Respectively, the resistance of an individual segment can be calculated as

$$R_j = \frac{\sum I_j}{I_j} R \tag{6}$$

The coefficients $r_j$ can be calculated from the measurement data using Equation 4 or by adding the anode activation to Equation 6. Here we used Equation 4 and the fitting results were analysed statistically.

The relation between the mass diffusion overpotential distribution and the current distribution can be calculated from Equations 1 and 4 as follows:

$$\eta_{conc,j} = E_{hom} - E + b\ln\left(\frac{i_{hom,j}}{i_j}\right) + r_j(i_{hom,j} - i_j) \tag{7}$$

### 2.2. *Fuel cell and measurement system*

The fuel cell assembly is the same as in our previous study [10], with the exception of the gas diffusion layer. Fuel cell components are listed in Table 1.

The 5 cm × 5 cm flow-field plate at the cathode side was divided into 48 segments, which were electrically insulated from each other. However, the MEA and gas diffusion layers were not segmented. The maximum error for local current densities resulting from this is in the range of 10% [10]. The plate had a total of 13 vertical flow channels, and the individual current collectors formed the ribs between the channels. The current collectors were made of gold-plated stainless steel. The channel pattern and the holes for the current collectors were machined into a PVC plate and an aluminium plate served as the endplate. The contact pressure between each current collector and the gas diffusion layer could be adjusted individually with two screws. The cross-section of the segmented measurement plate is illustrated in Figure 1.

*Table 1.* Description of the fuel cell components used in the measurements

| Component | Description | Manufacturer |
|---|---|---|
| Combined anode side end plate/current collector | 1 cm thick gold plated copper plate | Globe Tech, Inc. modified by authors |
| Anode side flow-field plate | Machined graphite plate for 25 cm$^2$ fuel cell, column flow pattern | Globe Tech, Inc. |
| Anode side gasket | 0.25 mm thick Teflon, reinforced with fiberglass | Oy ETRA Ab |
| Anode side gas diffusion layer | Carbon paper, Sigracet® GDL10-HM | SGL Carbon Group |
| MEA | Gore PRIMEA® | W.L. Gore and Associates |
| Cathode side gas diffusion layer | Carbon paper, Sigracet® GDL10-HM | SGL Carbon Group |
| Cathode side gasket | 0.25 mm thick Teflon, reinforced with fiberglass | Oy ETRA Ab |
| Combined cathode side flow-field plate/current collector/end plate | Straight open-to-air channel pattern [10] | Authors |
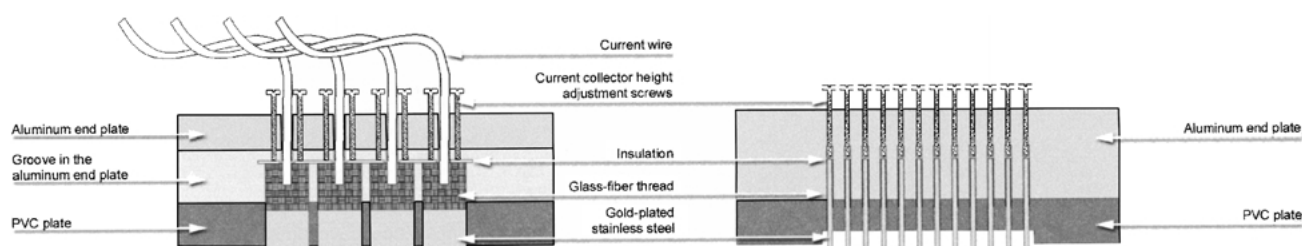


*Fig. 1.* Cross-sections from the segmented cathode flow-field plate. Left: vertical cut; right: horizontal cut.

The current from each segment was led through a 0.1 Ω precision resistor to a load unit. The voltage drop over each resistor was measured with a data logger. The time needed to record all of the voltage drops was approximately 2 s. The load unit featured a built-in current interrupter circuit for resistance measurements.

Dry hydrogen, with a purity of 99.999%, was fed to the anode from a pressure bottle. The minimum flow of hydrogen was set to 25 cm$^3$ min$^{-1}$ and for larger flows a relation 10 cm$^3$ min$^{-1}$ A$^{-1}$ $I$ (stoichiometry of 1.5), where $I$ is total current of the fuel cell, was used. The flow rate was controlled by a MKS type 1179A Mass-Flo® controller having an accuracy of ±5 cm$^3$ min$^{-1}$ in the range of 10–500 cm$^3$ min$^{-1}$. The hydrogen not consumed by the fuel cell was vented to the outside air.

The switch from the free-breathing to forced convection mode was made by feeding an airflow pulse to the bottom part of the cathode channels from a compressed air line. The flow rate of the airflow pulse was measured with a Compuflow Thermo-Anemometer GGA-65B. The accuracy of the anemometer was 1 m s$^{-1}$ in the range 21–30 m s$^{-1}$.

The flow rate exceeded the measurement range of the anemometer indicating that the flow rate of the airflow pulse was over 30 m s$^{-1}$ corresponding to a volumetric flow of 50 900 cm$^3$ min$^{-1}$. Thus, the airflow pulse used was highly over stoichiometric implying that no significant oxygen concentration gradients should occur in the cathode channels during the flow pulse. Moreover, the Reynolds number for the flow pulse should exceed 11 000 indicating turbulent flow. The turbulent flow enhances mass transfer inside the gas diffusion layer, which enables the formation of a uniform oxygen concentration not only in the gas channels but also in the electrode.

### 2.3. *Measurement procedure*

All measurements were conducted at ambient temperature (19 °C), pressure, and humidity (∼11%). The fuel cell was heated with a heating element positioned in the anode side end plate to a temperature of 30 °C. Before the polarization curve measurement, the fuel cell was allowed to stabilize at 100 mA cm$^{-2}$ current for 15 min. The polarization curve was measured starting at open circuit and ending at 180 mA cm$^{-2}$. The measurements were conducted using the cell in a galvanostatic mode, and the current step was set to 10 mA cm$^{-2}$ for $0 \leqslant i < 40$ mA cm$^{-2}$ and to 20 mA cm$^{-2}$ for larger currents. At each current, the cell was allowed to stabilize for 2 min and the current distribution was measured simultaneously. Immediately after this, a flow pulse was fed into the cathode channels for 10 s and the current distribution was again measured simultaneously. After the pulse, the fuel cell was allowed to stabilize for another 2 min before increasing the current.

## 3. Results

### 3.1. *Cell polarization*

The polarization curves for free and forced convection are depicted in Figure 2(a). The operation of the fuel cell was relatively stable up to 180 mA cm$^{-2}$ on free convection. Some voltage fluctuation was observed
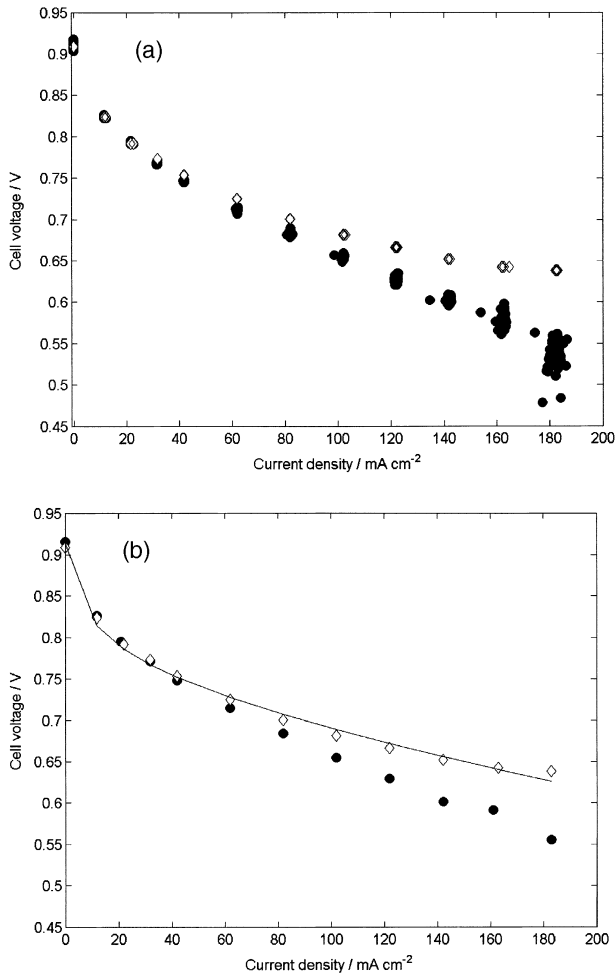
$$RMSD = \frac{\sqrt{\sum_{j} \left(E_{\text{calc,j}} - E_{\text{meas,j}}\right)}/n}{\sum_{j} \left(E_{\text{meas,j}}\right)/n} \qquad (9)$$

where $n$ is the number of data points. The *MBD* was 1.3% and the *RMSD* was 0.2%, which indicates good fitting.

### 3.2. *Current distributions*

Current distributions for free and forced convection were measured simultaneously with the polarization measurement. The measured points of each segment were averaged for each current density level. The distributions from the current densities of 60, 100, 140 and 180 mA cm$^{-2}$ are depicted in Figure 3. In each figure, the distribution on the left is from the forced convection measurement and the one on the right is from the free convection measurement. The bottom of the fuel cell lies on the row $y = 1$ and the top on the row $y = 4$. Hydrogen was fed to the cell from the corner $x = 1$ and $y = 4$ (from now on referred to as pin (1,4)) and vented out from (12,4).

The contact pressure between the pin (4,1) and the gas diffusion layer was allowed to be lower than for the rest of the pins so that the method could be verified even for a nonuniform contact resistance distribution. This explains the pronounced drop in each figure.

Because of the 0.1 $\Omega$ measurement resistors, the cathode segments of the fuel cell are polarized slightly differently. This causes some error to the resistance and mass diffusion overpotential distributions because the potential of each segment was assumed to be the same in Equations 4–7. The maximum difference in the current densities between the segments is obtained with free convection at 180 mA cm$^{-2}$ causing 10 mV voltage deviation between the measurement pins (1,4) and (6,1). The unequal polarization of the measurement pins smoothes the current density distributions and thus also the resistance and mass diffusion overpotential distributions. However, the nonsegmented gas diffusion layer decreases the effect of polarization caused by the measurement resistors and thus decreases the polarization.

The distributions obtained from the forced convection measurement remained in shape throughout the current range since the standard deviation of the relative change in each current density distribution compared to the distribution at 60 mA cm$^{-2}$ is about 1%. This can also be seen from the current distribution (Figure 3). The unchanging shape implies that the duration of the flow pulse (10 s) was adequate to form a uniform oxygen concentration over the entire electrode area, and the resistance of the proton conductive phases did not change during the measurement. However, the shape of the distribution measured in free convection changes radically during the current scan. At low current densities, the distribution is quite uniform but at higher
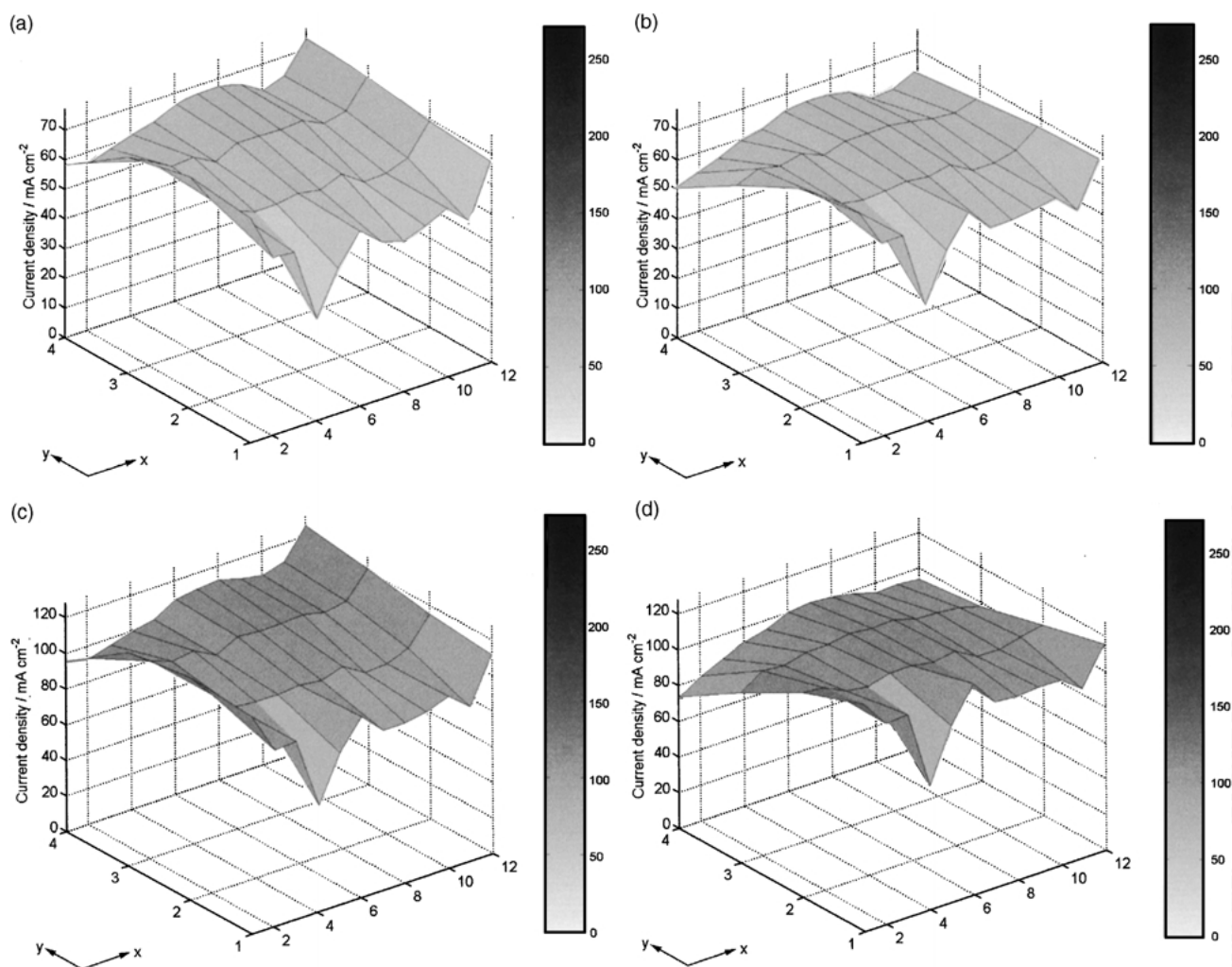
*Fig. 2.* (a) Measured cell polarization curves; (b) average polarization curves (bullets) with a fitted polarization curve on forced convection data (line). Air supply: free convection ($\bullet$) and forced convection ($\diamond$).

at high current densities, which may cause some error. However, the standard deviation of the voltage at 180 mA cm$^{-2}$ was about 0.01 V (average voltage 0.54 V), which indicates that the fuel cell was in steady state operation. The operation of the cell on forced convection was stable throughout the measurement.

The averaged polarization curves and the Tafel equation fitted to the forced convection data are shown in Figure 2(b). The fitting was made using the nonlinear least square sum method yielding fitting coefficients $E_0 = 0.914$ V, $b = 0.0378$ V dec$^{-1}$ and $r = 0.497\,\Omega$ cm$^2$. These are of the same order of magnitude as in [11]. The error resulting from the least squares fitting was analysed with the relative mean bias difference *MBD* and the relative root mean square difference *RMSD*. The *MBD* can be expressed as

$$MBD = \frac{\sum_{j} \left(E_{\text{calc,j}} - E_{\text{meas,j}}\right)/n}{\sum_{j} \left(E_{\text{meas,j}}\right)/n} \qquad (8)$$

and the *RMSD* as

*Fig. 3.* Current distributions at average current densities: (a) forced convection at 60 mA cm$^{-2}$ (0.72 V); (b) free convection at 60 mA cm$^{-2}$ (0.71 V); (c) forced convection at 100 mA cm$^{-2}$ (0.68 V); (d) free convection at 100 mA cm$^{-2}$ (0.65 V); (e) forced convection at 140 mA cm$^{-2}$ (0.65 V); (f) free convection at 140 mA cm$^{-2}$ (0.60 V); (g) forced convection at 180 mA cm$^{-2}$ (0.64 V); (h) free convection at 180 mA cm$^{-2}$ (0.55 V).

currents the bottom of the cell operates noticeably better. This indicates increased mass diffusion overpotential in the upper parts of the cell.

### 3.3. *Cell resistance and resistance distribution*

The resistance of the fuel cell in the free and forced convection measurements is illustrated in Figure 4(a), We have shown previously [12] that the accuracy of resistance readings decreases at current densities below 100 mA cm$^{-2}$. Furthermore, some additional error throughout the current density range may result in the resistance readings due to the slowness of the current interruption measurement equipment and the capacitance of our cell. However, the resistance measurement is accurate enough for qualitative conclusions to be made. It can therefore, be determined that the duration of the flow pulse (10 s) was sufficient short, since the resistance of the cell did not change during the flow pulses.

The fitting coefficients $r_j$ are depicted in Figure 4(b) These were calculated for each pin using Equation 4 by assuming that the activation overpotential of the cathode and the exchange current density did not change during the flow pulse. Thus, the same coefficients for $E_0$ and $b$ as before were used.

The resistance distributions calculated from Equation 6 are illustrated in Figure 5 for current densities of 60, 100, 140 and 180 mA cm$^{-2}$. The high contact resistance of the pin (4,1) is clearly seen. It can also be seen that the resistance is slightly increased at the hydrogen inlet (1,4). When dry hydrogen is used on the anode, some drying of the proton conductive phases may take place. Similar behaviour has been seen in our previous measurements [10]. It should be also noticed that the nonsegmented gas diffusion layer and the measurement resistors have a smoothing effect on the resistance distribution.

The *MBD* values were calculated for fitting coefficients $r_j$ and resistance distributions for different current levels to see how well the distribution of $r_j$ follows the resistance distributions. Results are given in Table 2.
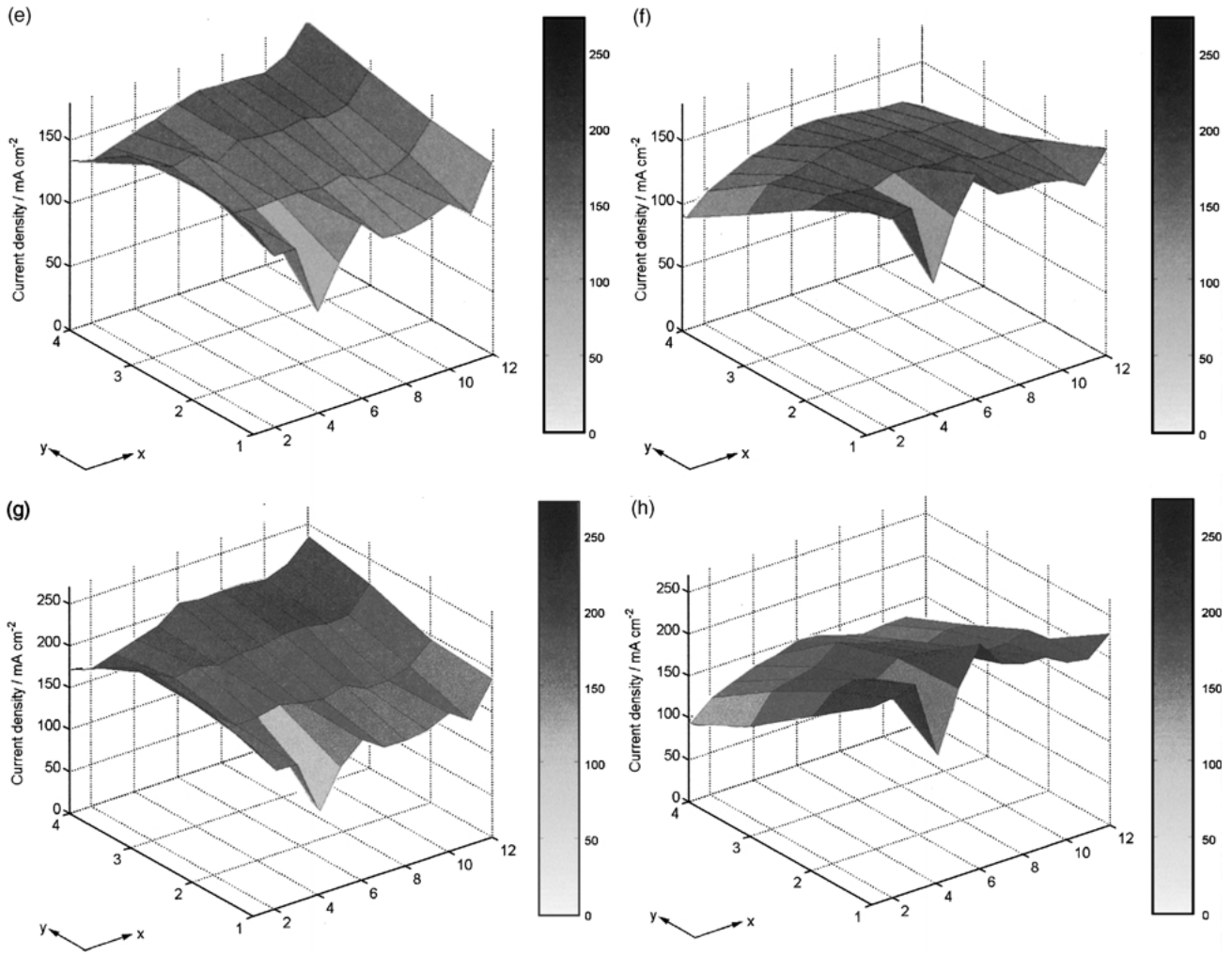
(e)

(f)

(g)

(h)

Fig. 3. (Continued)



(a)

(b)
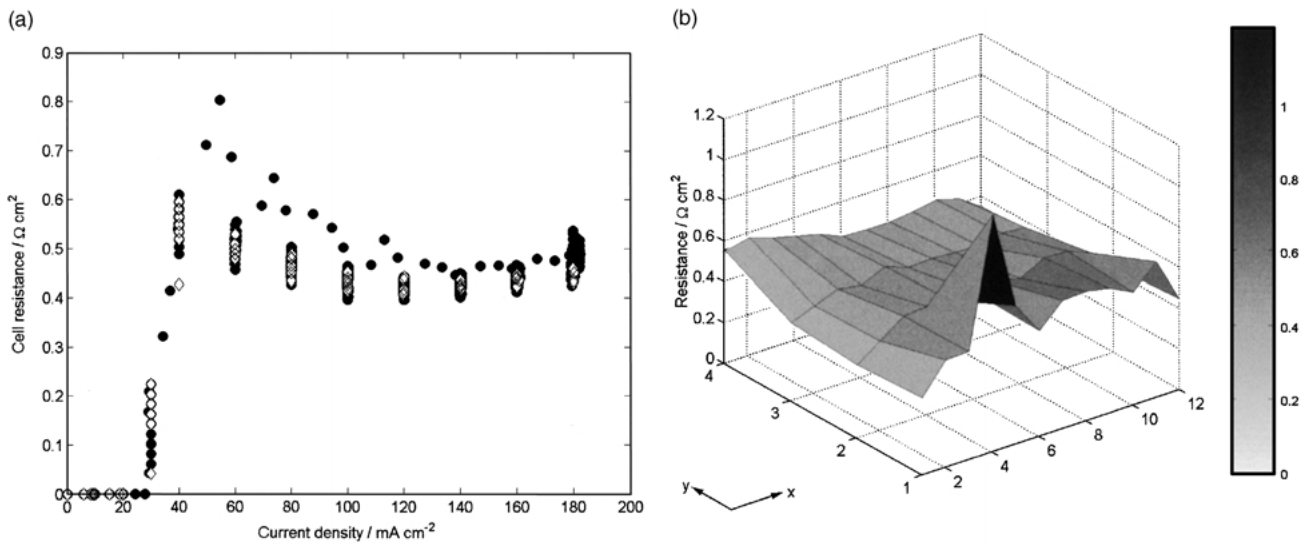
Fig. 4. (a) Cell resistances as a function of current density at free convection (●) and forced convection (◇); (b) the fitting coefficients $r_j$.

It appears that the fitting coefficients $r_j$ are generally overestimated according to the *MBD* calculation. This was an expected result because the measured cell resistance does not take the anode activation overpotential into account. The differences in the *MBD* values result from inaccuracies in the resistance readings; the
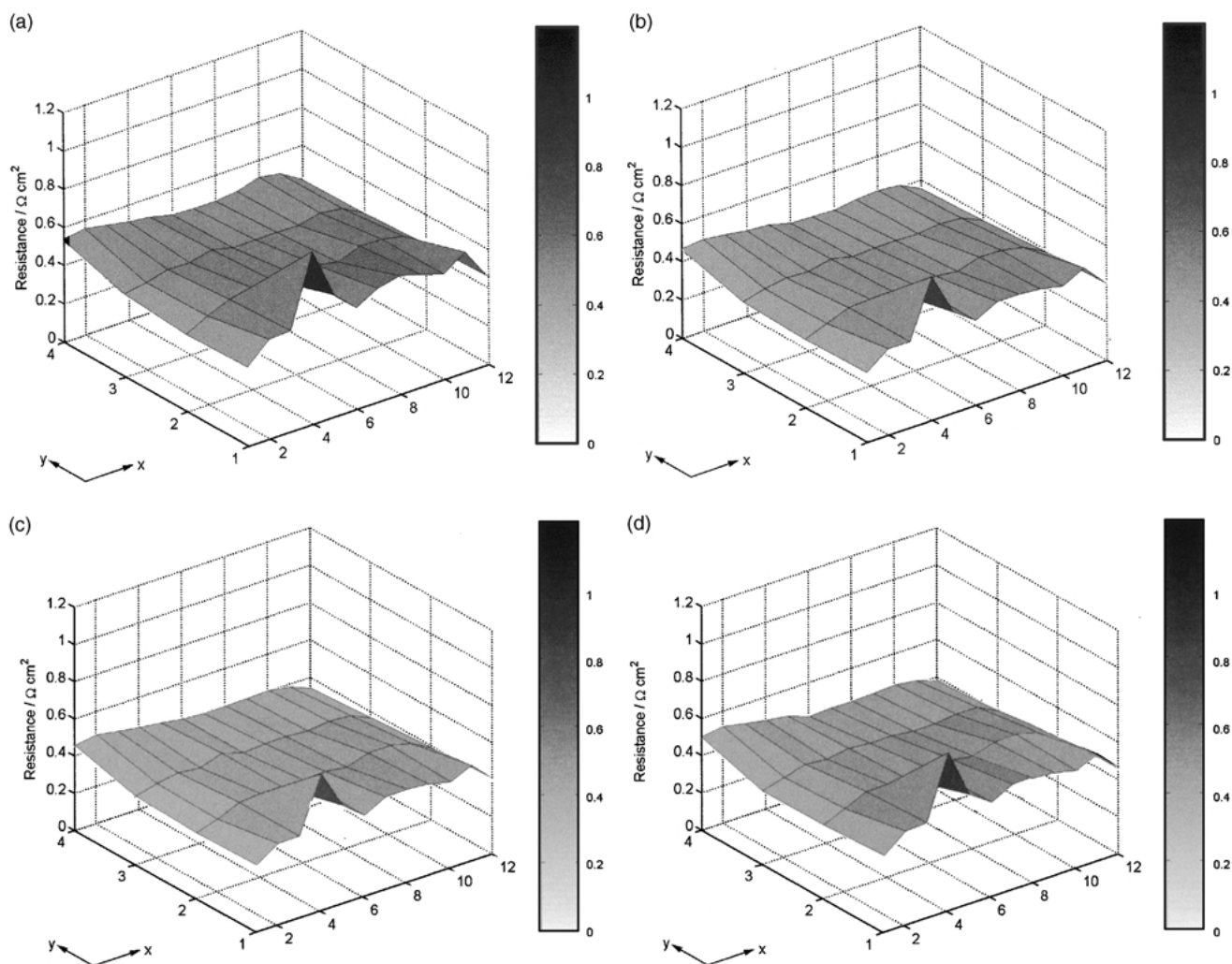
*Fig. 5.* Resistance distributions at average current densities: (a) 60, (b) 100, (c) 140 and (d) 180 mA cm$^{-2}$.

*Table 2.* MBD of the resistance distributions and fitting coefficients $r_j$ at different current levels

| Average current density /mA cm$^{-2}$ | MBD /% |
|---|---|
| 60 | −0.2 |
| 80 | 8.1 |
| 100 | 15.5 |
| 120 | 19.3 |
| 140 | 18.6 |
| 160 | 14.5 |
| 180 | 6.7 |

measurement system overestimated the cell resistance at low current densities, and the cell resistance was slightly increased at high current densities.

### 3.4. *Mass diffusion overpotential distributions*

The mass diffusion overpotentials for each segment were calculated using Equation 7 and the results are depicted in Figure 6 for average current densities of 60, 100, 140 and 180 mA cm$^{-2}$. The effect of the mass diffusion

overpotential is pronounced at the top sections and edges of the cell. Because the airflow direction in the cathode side channels is upwards due to the molecular diffusion and temperature buoyancy, the bottom parts of the fuel cell have the highest oxygen concentration, resulting in a low diffusion overpotential. The increased mass diffusion overpotential at the edges may imply that the temperature distribution of the cell is uneven and the temperature is higher in the central parts of the cell.

The mass diffusion overpotential distribution in the vertical direction is notable at each current level but is emphasized with increased currents. The average difference (edges not included) of the mass diffusion overpotential between the bottom and top parts of the cell at 60 mA cm$^{-2}$ is only 0.010 V, and the average difference at 180 mA cm$^{-2}$ is 0.10 V. It should be noticed that the nonsegmented gas diffusion layer and the measurement resistors smooth the mass diffusion overpotential distributions and thus the real distributions ought to be somewhat more pronounced.

The mass diffusion overpotentials determined directly from the measurement, the mass diffusion overpotentials calculated from the fitted data, and their *MBD* are
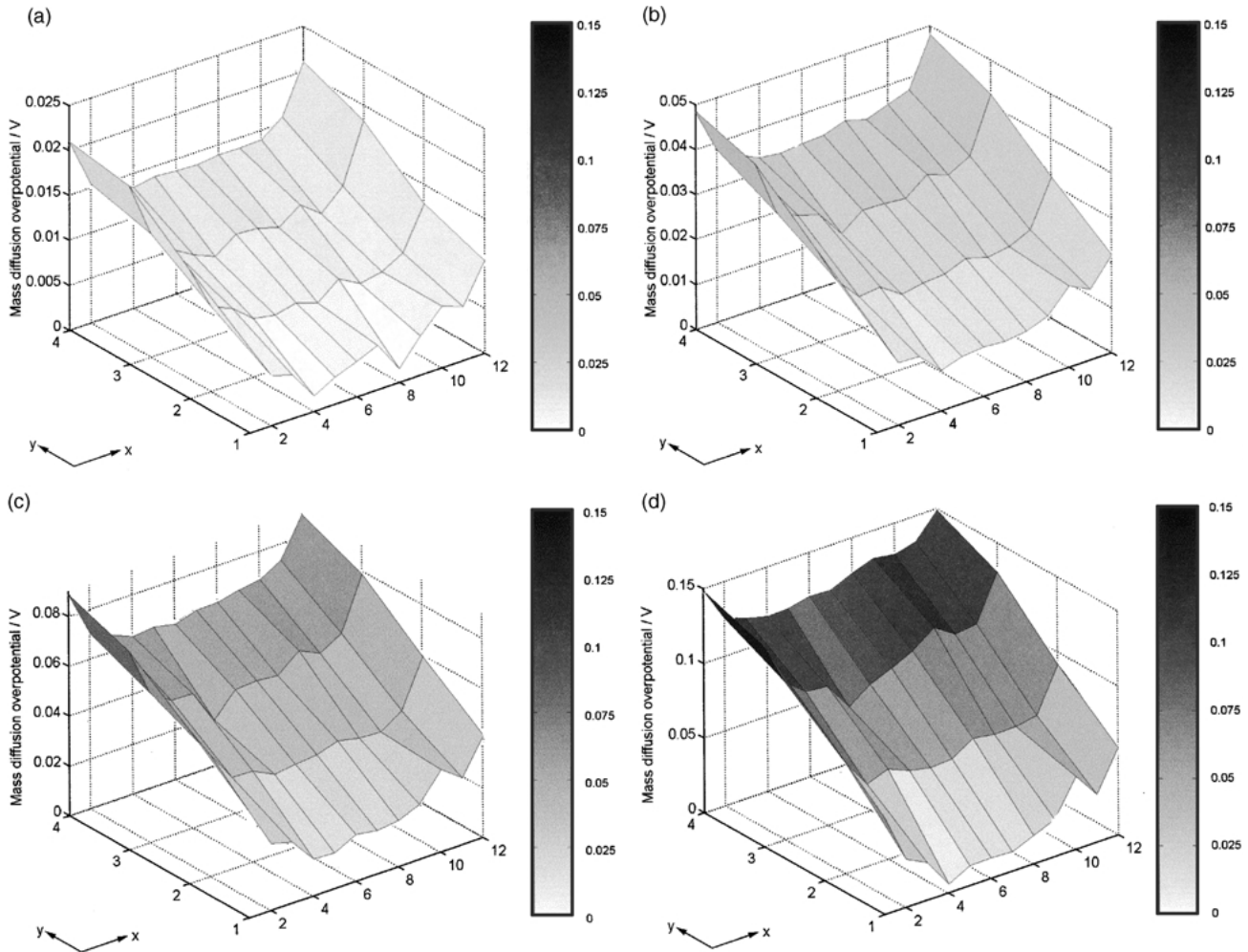
*Fig. 6.* Mass diffusion overpotential distributions at average current densities: (a) 60, (b) 100, (c) 140 and (d) 180 mA cm$^{-2}$.

given in Table 3. The mass diffusion overpotential determined directly from the measurement is calculated as the difference between the forced and free convection measurement results, whereas the mass diffusion overpotential calculated from the fitted data is calculated as an average over the segments.

It can be seen that the error resulting from the fitting is relative small, only about 3–4%. In addition, it can be seen that the calculation always underestimates the mass diffusion overpotential because the *MBD* is negative.

*Table 3.* Measured and average of the fitted mass diffusion overpotentials (MDO) and their MBD at different current levels

| Average current density /mA cm$^{-2}$ | Measured MDO /V | Fitted MDO /V | MBD /% |
|---|---|---|---|
| 60 | 0.010 | 0.0099 | −3.9 |
| 80 | 0.017 | 0.016 | −3.5 |
| 100 | 0.026 | 0.026 | −1.9 |
| 120 | 0.036 | 0.035 | −3.2 |
| 140 | 0.050 | 0.049 | −3.0 |
| 160 | 0.051 | 0.050 | −2.7 |
| 180 | 0.084 | 0.081 | −3.2 |

The most significant factor in the difference resulted from the use of coefficients $r_j$, which were kept constant at each current density level, although the cell resistance changed during the measurement.

## 4. Conclusions

An approach to determine the mass diffusion overpotential distribution in a PEM fuel cell is presented. The approach has been developed for a free-breathing fuel cell but can also be utilized for other kinds of PEMFC. Highly over stoichiometric flow pulses were fed to the cathode channels to form homogenized oxygen concentration along the reaction surface. Simultaneously, the current distribution and cell resistance was measured. The current distribution was measured with a segmented flow-field plate and the cell resistance with the current interruption method. A modified Tafel equation was used to determine the mass diffusion overpotential for each cell segment.

The cell resistance distribution was also determined from the experimental data. Even though the resistance distribution was somewhat non-uniform, the results

showed that the high contact resistance of one of the measuring pins did not affect the experimental mass diffusion overpotential distribution.

At small current densities, the mass diffusion overpotential distribution was insignificant as expected, for example at 60 mA cm$^{-2}$ the difference in the 5 cm long channel between the bottom and top part of the cell was only about 0.01 V. However, the proportion of the mass diffusion overpotential in the losses increased at higher current densities and also the mass diffusion distribution became more uneven. At a current density of 180 mA cm$^{-2}$, the mass diffusion overpotential difference between the bottom and top part of the cell was about 0.1 V. This highlights the significance of mass diffusion overpotential resulting from the use of free convection. However, the results indicate that the efficiency of the cell can be improved significantly by reducing the length of the cathode channels.

## Acknowledgements

## References

1. Z.H. Wang, C.Y. Wang and K.S. Chen, *J. Power Sources* **94** (2001) 40.
2. D. Natarajan and T.V. Nguyen, *J. Electrochem. Society* **148** (2001) A1324.
3. S.J.C. Cleghorn, C.R. Derouin, M.S. Wilson and S. Gottesfeld, *J. Appl. Electrochem.* **28** (1998) 663.
4. J. Stumper, S.A. Campbell, D.P. Wilkinson, M.C. Johnson and M. Davis, *Electrochim. Acta* **43** (1998) 3773.
5. Ch. Wieser, A. Helmbold and E. Gulzow, *J. Appl. Electrochem.* **30** (2000) 803.
6. Ch. Wieser, A. Helmbold and W. Schnurnberger, *Proc. Electrochem. Soc.* **98–27** ('Proton Conducting Membrane Fuel Cells II') (1999) 457.
7. A.R. Kucernak, N.P. Brandon, V. Vesovic, S. Atkins, D.J.L. Brett and N. Vasileiadis, Proceedings of the 1st European PEFC Conference (2001), p. 297.
8. D.J.L. Brett, S. Atkins, N.P. Brandon, V. Vesovic, N. Vasileiadis and A.R. Kucernak, *Electrochem. Commun.* **3**(11) (2001) 628.
9. C. Hebling, M. Zedda, A. Schmitz, U. Groos, A. Hakenjos, J. Schumacher and K. Tüber, Fraunhofer Institut Solare Energiesysteme, 'Annual Report 2000' (2001), p. 52.
10. M. Noponen, T. Mennola, M. Mikkola, T. Hottinen and P. Lund, *J. Power Sources* **106** (2002) 304.
11. G. Squadrito, G. Maggio, E. Passalacqua, F. Lufrano and A. Patti, *J. Appl. Electrochem.* **29** (1999) 1449.
12. M. Mikkola, 'Experimental Studies on Polymer Electrolyte Membrane Fuel Cell Stacks', Master's thesis, Helsinki University of Technology (2001).